Hydromagnetic Flow of Casson Fluid Carrying CNT and Graphene Nanoparticles in Armory Production

ABAYOMI S. OKE[1], BELINDAR A. JUMA[2], ANSELM O. OYEM[3]
[1]Department of Mathematical Sciences,
Adekunle Ajasin University, Akungba Akoko,
NIGERIA

[2]Department of Mathematics,
University College London,
UNITED KINGDOM

[3]Department of Mathematics,
Busitema University,
UGANDA

**Corresponding Author*

Abstract: - Carbon nanotubes (CNTs) and graphenes possess the properties that make them the future of armory in the military. Bullet-proof vests, for instance, are indispensable components of any military arsenal whose maintenance cost and weight can be drastically reduced if the materials are changed to CNT and graphenes. The purpose of this study is to investigate heat and mass transport phenomena in the hydromagnetic flow of Casson fluid suspending carbon nanotubes and graphene nanoparticles in armory production. An appropriate model is developed, taking into account the Buongiorno model and the effect of heat radiation. Using similarity variables, the model is reformulated into a dimensionless form. The numerical solution to the dimensionless model is obtained using the three-stage Lobatto IIIa finite difference approach, which is programmed into the MATLAB bvp4c package. The study reveals that an increase in the Casson fluid parameter leads to a decrease in the velocity profiles. There is a 78.41% reduction in skin friction when results are compared with the CNT-water nanofluid.

Key-Words: - Hydromagnetic, MHD, Heat and mass transfer, CNTs, Graphene, Casson fluid, Hybrid nanofluid

Received: November 18, 2022. Revised: August 27, 2023. Accepted: October 6, 2023. Published: November 8, 2023.

1 Introduction

Most natural and engineered fluids do not obey the Newtonian law of viscosity, [1], [2], [3], [4]. These diverse properties of the fluids led to the formulation of fluid models such as the Casson fluid model, the Carreau fluid model, and the Williamson fluid model, [5], [6], [7], [8], [9]. The Casson fluid model is of major medical importance due to its ability to model the flow of blood, [10]. The study, [11], mathematically analyzed the Casson fluid model and the results are in agreement with rheological results on blood. The search for a better thermally conducting fluid was initiated by, [12], when he added millimetre-scale solid particles to a fluid. The study, [13], however, improved on the work by proposing nanoparticles in place of the millimeter-sized solid particles. The resulting suspension of nanoparticles in a base fluid is now called nanofluids. Nanofluids have a lot of applications in different industrial and technological areas due to their enhanced heat transfer rate, [14], [15], [16]. The study, [17], proposed the class hybrid nanofluids, in which two nanoparticles are suspended in a base fluid. It was shown that the hybrid nanofluid possesses better properties compared with the individual nanofluids. Of many important properties that can be studied in hybrid nanofluid flow, the rate of heat transmission is of prime importance. This prompted, [18], to develop a mathematical model to study the improvement of heat transfer in $Ag-CuO$ hybrid nanofluids with water-based fluid. The results indicated an improvement in the heat transmission of the hybrid nanofluid compared to nanofluids and ordinary fluids, [19], [20], [21]. The study, [22], proceeded to carry out a theoretical comparison between the heat transmission of a hybrid micropolar nanofluid and

the heat transmission of the micropolar nanofluid. The results inferred the best heat transmission rate is found in the hybrid micropolar fluid. The study, [23], reiterated that heat transmission is drastically improved in hybrid nanofluid when compared with the ordinary base fluid or a nanofluid of similar individual nanoparticles. The study, [24], explored the semi-analytical solutions of an unsteady flow of a hybrid nanofluid and their results showed the existence of one stable solution and one unstable solution. The study, [25], explained the existence of the two solutions by showing that only one of the solutions is significant for the research study. The other solution is only useful for mathematical completeness. The study, [26], took a more detailed look into the flow of a hybrid nanofluid with an incompressible base fluid in a rotating disk. After a detailed analysis of different pairs of nanoparticles in the base fluid, they concluded that some nanoparticles like Carbon nanotubes greatly improve the heat transfer rate than many others. The study, [27], elucidated the significance of magnetic field strength and heat source on the flow of hybrid nanofluid over an exponential stretching Surface (ESS). More recently, [28], studied heat and mass transfer flow in the flow of Casson nanofluid in a mixed-convective double diffusive flow with convective boundary conditions. The result indicated that skin friction, heat transfer rate, and Sherwood number are enhanced with increasing Biot number.

Steel, aramids, and Polypyridobisimidazole (PIPD) are the most common materials used in armory fabrication. Bullet-proof vests are now made from stiff and durable fibers that are woven and laminated securely in layers. The fabric material absorbs the energy of the impacting bullet by stretching the fibers, and the stiff fibers guarantee that the load is distributed across a vast area within the material. This mechanism slows the bullet and eventually prevents it from hitting the body. The ability of a fiber to deform in polymer matrix composites (PMCs) is severely limited as a result of surrounding resin, and therefore the energy absorption capacity is diminished. Under ballistic impact, the predominant failure modes in PMCs include fiber strain and fracture, delamination, and shear deformation in the resin matrix, [29]. The strength of graphenes and carbon nanotubes, as well as their extremely lightweight, high thermal and electrical conductivities, elasticity, high tensile strength, and low thermal expansion coefficient, contribute to their potential ability to replace current materials used in the production of armories. Furthermore, graphenes and carbon nanotubes enable the creation of wearable computers, lightweight bullet-proof jackets, and a less expensive alternative to military aircraft, [30], [31].

This research is designed to analyze the heat and mass transfer in a Casson hybrid nanofluid flow across an exponentially stretching sheet. The choice of CNT and graphene nanoparticles is due to their outstanding heat and electrical conductivity, aspect ratio, [32], and lightweight which makes them the best alternative to armory productions and heat exchange performance. By combining these two great materials, it is hoped that they enhance heat transfer in the flow of electrically conducting Casson hybrid nanofluid. This study provides answers to the following questions;

1. How does radiation and haphazard motion of the fluid particles affect the flow velocity of the hybrid nanoparticles?
2. In what ways does the variation in volume fraction influence the flow temperature of the hybrid nanofluid suspending CNT and Graphene nanoparticles?
3. What are the impacts of Magnetic parameters on the flow velocity, temperature, and concentration of the hybrid nanofluid suspending CNT and Graphene nanoparticles?

2 Governing Equations

The physical configuration of the flow is depicted in Figure 1. A Casson base fluid is chosen for this study in which CNT and Graphene nanoparticles are suspended. The resulting hybrid nanofluid flows across a surface in which a magnetic field is applied normally to the flow. The magnetic field is assumed to have a constant magnetic field strength B_0. The surface is stretching exponentially in the x-direction so that the fluid layers adjacent to the wall have the same stretching velocity $u = U_0 e^{x/L}$. The flow is steady, incompressible, two dimensional and the no-slip condition is considered.

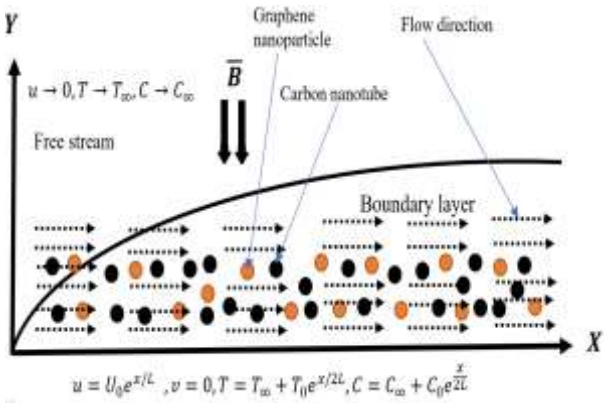

Fig. 1: Flow configuration

Adopting the Buongiorno model to correct the dimensionless units in, [33], and after the boundary layer analysis, [34], equations governing the flow of Casson hybrid nanofluid over an ESS in the presence of thermal

$$\frac{\partial u}{\partial x}+\frac{\partial v}{\partial y}=0, \tag{2.1}$$

$$u\frac{\partial u}{\partial x}+v\frac{\partial u}{\partial y}=\left(1+\frac{1}{\gamma}\right)\frac{\mu_{hnf}}{\rho_{hnf}}\frac{\partial^2 u}{\partial y^2}+g\beta(T-T_\infty)-\frac{\sigma_{hnf}}{\rho_{hnf}}B_0^2 u, \tag{2.2}$$

$$u\frac{\partial T}{\partial x}+v\frac{\partial T}{\partial y}=\alpha_{hnf}\frac{\partial^2 T}{\partial y^2}+\frac{1}{(\rho C_p)_{hnf}}\frac{\partial q}{\partial y}+\tau\left(\frac{D_B}{\Delta C}\frac{\partial C}{\partial y}\frac{\partial T}{\partial y}+\frac{D_T}{T_\infty}\frac{\partial T}{\partial y}\frac{\partial T}{\partial y}\right), \tag{2.3}$$

$$u\frac{\partial C}{\partial x}+v\frac{\partial C}{\partial y}=D_B\frac{\partial^2 C}{\partial y^2}+\frac{D_T\Delta C}{T_\infty}\frac{\partial^2 T}{\partial y^2}. \tag{2.4}$$

subject to the no-slip boundary and initial conditions

$$\text{at } y=0: u=U_0e^{\frac{x}{L}}, v=0, T=T_\infty+T_0e^{\frac{x}{2L}}, C=C_\infty+C_0e^{\frac{x}{2L}} \tag{2.5}$$

$$\text{as } y\to\infty: u\to 0, \quad T\to T_\infty, C\to C_\infty. \tag{2.6}$$

where all variables are as defined in the nomenclature and adopting the formulation in, [9],

$$\frac{\partial q}{\partial y}=\frac{16\sigma^*T_\infty^3}{3K^*}\frac{\partial^2 T}{\partial y^2}.$$

3 Methodology

The appropriate similarity variables for the system of equations (2.1 - 2.4) with the boundary conditions (2.5 - 2.6) are

$$\eta=y\left(\frac{U_0}{2\nu_f L}\right)^{\frac{1}{2}}\exp\left(\frac{x}{2L}\right),\quad u=U_0\exp\left(\frac{x}{2L}\right)f',$$

$$v=-\left(\frac{U_0\nu_f}{2L}\right)^{\frac{1}{2}}\exp\left(\frac{x}{2L}\right)[\eta f'+f],$$

$$T=T_\infty+T_0\exp\left(\frac{x}{2L}\right)\Theta,$$

$$C=C_\infty+C_0\exp\left(\frac{x}{2L}\right)\Phi.$$

Setting

$$A_1=\frac{(1-\phi)^{-\frac{5}{2}}}{1-\phi+\phi_1\frac{\rho_1}{\rho_f}+\phi_2\frac{\rho_2}{\rho_f}},$$

$$A_2=\frac{\left\{\frac{(1+2\phi)(\phi_1K_1+\phi_2K_2)+2(1-\phi)\phi K_f}{(1-\phi)(\phi_1K_1+\phi_2K_2)+(2+\phi)\phi K_f}\right\}}{\left\{(1-\phi)+\frac{\phi_1(\rho C_\rho)_1}{(\rho C_\rho)_f}+\frac{\phi_2(\rho C_\rho)_2}{(\rho C_\rho)_f}\right\}}$$

and defining the dimensionless parameters

$$Gr=\frac{Lg\beta T_0e^{-\frac{3x}{2L}}}{U_0^2},\quad M=\frac{L\sigma_{hnf}B_0}{U_0\rho_{hnf}}e^{-\frac{x}{L}},$$

$$Sc=\frac{\nu_f}{D_B},\quad Pr=\frac{\nu_f}{\alpha_f},\quad R=\frac{4\sigma^*T_\infty^3}{K^*K_{hnf}},$$

$$N_t=\frac{D_T}{T_\infty}\frac{T_0}{\alpha_f}\tau e^{\frac{x}{2L}},\quad N_b=\frac{D_B}{\Delta C}\frac{C_0}{\alpha_f}\tau e^{x/2L},$$

Then the dimensionless forms of the system of equations (2.1 - 2.4) are

$$\left(1+\frac{1}{\gamma}\right)A_1f'''+2Gr\Theta-2Mf'-2(f')^2+ff''=0 \tag{3.1}$$

$$A_2\left(1+\frac{4}{3}R\right)\Theta''+N_b\Theta'\Phi'+N_t(\Theta')^2-Pr\Theta f'+Pr\Theta' f=0 \tag{3.2}$$

$$\Phi''+\frac{N_t}{N_b}\Theta''+Scf\Phi'-Scf'\Phi=0. \tag{3.3}$$

with the boundary conditions

$$\text{for } \eta=0;\ f'=1;\ f=0;\ \Theta=1;\ \Phi=1 \tag{3.4}$$

$$\text{as } \eta\to\infty;\ f'\to 0;\ \Theta\to 0;\ \Phi\to 0; \tag{3.5}$$

Rewriting the dimensionless equations as a system of first-order ODEs, we have;

$$u_1'=u_2, \tag{3.6}$$

$$u_2'=u_3, \tag{3.7}$$

$$u_3'=-\frac{2Gru_4-2Mu_2-2u_2^2+u_1u_3}{\left(1+\frac{1}{\gamma}\right)A_1}, \tag{3.8}$$

$$u_4'=u_5, \tag{3.9}$$

$$u_5'=-\frac{N_bu_5u_7+N_tu_5^2-Pru_4u_2+Pru_5u_1}{A_2\left(1+\frac{4}{3}R\right)}, \tag{3.10}$$

$$u_6'=u_7 \tag{3.11}$$

$$u_7'=-\left(\frac{N_t}{N_b}u_5'+Scu_1u_7-Scu_2u_6\right) \tag{3.12}$$

with boundary conditions given as

$$u_2(0)=1;\ u_1(0)=0;\ u_4(0)=1;\ u_6(0)=1 \tag{3.13}$$

$$u_2(\infty)\to 0;\ u_4(\infty)\to 0;\ u_6(\infty)\to 0. \tag{3.14}$$

and

$$u_1=f,\quad u_2=f',\quad u_3=f'',\quad u_4=\Theta,\quad u_5=\Theta',\quad u_6=\Phi,\quad u_7=\Phi'$$

The quantities of practical interest are the coefficient of skin friction, Nusselt number, and Sherwood number given as

$$C_f=\frac{\tau_w}{\rho_fU_0^2},$$

$$N_u=\frac{xq_w}{K_{hnf}(T_w-T_\infty)},$$

$$S_h=\frac{xJ_w}{D_B(C_w-C_\infty)},$$

where

$$\tau_w = \mu_{hnf}\left(1+\frac{1}{\gamma}\right)\frac{\partial u}{\partial y}\Big|_{y=0},$$
$$q_w = -K_{hnf}\frac{\partial T}{\partial y}\Big|_{y=0},$$
$$J_w = -D_B\frac{\partial C}{\partial y}\Big|_{y=0}.$$

The dimensionless form of the quantities of interest are

$$C_f Re^{1/2} = \left(1+\tfrac{1}{\gamma}\right)f''(0),$$
$$N_u Re^{-1/2} = -\Theta'(0),$$
$$Re^{-1/2}S_h = -\Phi'(0).$$

In this study, the Shooting Technique is employed to convert the dimensionless boundary value problem above to its equivalent initial value problem. The conditions (3.13) and (3.14) are written as

$$u_1(0)=0;\ u_2(0)=1;\ u_3(0)=r_1;\ u_4(0)=1; \quad (3.15)$$
$$u_5(0)=r_2;\ u_6(0)=1;\ u_7(0)=r_3; \quad (3.16)$$

and solve the system of equations (3.6 - 3.12) with some initial guesses for r_1, r_2, r_3 and the results are compared with the three free stream conditions (3.14). The guesses are updated based on errors found in the comparison. The process is repeated until a tolerable error is achieved. Once the equivalent initial value ordinary differential equation has been obtained, then the 3-stage Loabtto IIIa is executed to solve the problem (Other methods of solution can be found in, [35]). The Lobatto IIIa method is a symmetric and nonstiff A-stable method whose stability function $R(z)$ is $(s-1, s-1)$-Pade approximation to e^z. By setting $N_b = N_t = Sc = 0$, and $\gamma \to \infty$ in the present work and setting $\epsilon = \lambda = s = 0$ in, the two models coincide. The results from this study are therefore compared with the outcomes of, [17], as shown in Table 1 and it shows that there is a good agreement between the results from this present study and the work of, [17].

Table 1. Validation of results

Pr	*M*	*R*	[17]	Present work
0.5	0	0	0.5967	0.5965
1	0	0	0.9548	0.9548
2	0	0	1.4715	1.4714
1	1	0	0.8615	0.8615
1	1	1	0.4620	0.4619
25	1	1	1.2016	1.2016

4 Analysis and Discussion of Results

Equations (3.6 - 3.14) are solved using MATLAB bvp4c with a tolerance level of 10^{-6} and the following default values of the parameters are chosen

$$Gr = M = N_b = N_t = 1;\ \gamma = 10;\ Pr = 7;$$
$$R = 2;\ Sc = 0.63;\ \phi_1 = \phi_2 = 0.15.$$

The results from the simulations are depicted as graphs. The thermophysical properties of the nanoparticles and the base fluid are shown in Table 2.

Table 2. Thermophysical properties

	ρ	c_p	K_1	Source
SWCNT	2600	425	6600	[36]
Graphene	2250	2100	2500	[37]
Blood	1093	3210	0.451	[38]

4.1 Effects of Various Parameters on the Velocity Profile

The effects of the various dimensionless parameters on the velocity profiles are shown in Figure 2, Figure 3, Figure 4 and Figure 5. Figure 2 shows that increasing the Casson parameter causes a decrease in the primary velocity. Increasing the Casson fluid parameter leads to an increase in the viscous boundary layer thickness thereby increasing the viscous effects in the flow. The presence of a magnetic field in the flow field generates an impeding force known as the Lorentz force. The Lorentz force opposes fluid flow and increasing the magnetic field strength implies an increase in the Lorentz force. This explains why increasing magnetic field strength reduces the velocity profiles. Figure 3 shows the decrease in primary velocity with increasing Magnetic parameters. The continuous collision of the suspended nanoparticles with each other and the wall of the stretching surface leads to increased kinetic energy in the flow which in turn leads to an increase in the velocity profiles (Figure 4). Furthermore, increasing the Radiation parameter increases heat energy in the flow. The influx of heat excites the fluid particles which increases the flow velocity. Hence, there is a notable increase in the velocity profiles when the Radiation parameter is increased (Figure 5).

4.2 Effects of Various Parameters on the Temperature Profiles

As the Casson fluid parameter increases to infinity, the fluid becomes Newtonian. Hence, increasing the

Casson fluid parameter leads to an increase in the thermal boundary layer thickness, which in turn creates a surge in the temperature gradient. This explains why the temperature profile increases with increasing Casson fluid parameters as shown in Figure 6. Figure 7 shows that increasing the Magnetic field parameter increases the temperature profile. This observation can be traced to the fact that the Lorentz force generated from the magnetic field creates a lot of internal friction between the fluid molecules within the thermal boundary layer. Additional internal energy is created in the form of heat which raises the flow temperature profiles as magnetic field strength increases. An increase in the volume fraction increases the surface area of the nanoparticles which enhances an improved thermal conductivity. Therefore, as expected, Figure 8 shows an increase in the volume fraction increases the temperature profile. The increase in the temperature profile in Figure 9 is a result of the increasing thermal radiation.

4.3 Effects of Various Parameters on the Concentration Profile

Figure 10, Figure 11 and Figure 12 illustrate the effects of the dimensionless parameters on the concentration. As the Casson parameter γ increases, the concentration profile increases due to the increase in the concentration at the boundary layer (as shown in Figure 10). Increasing the magnetic field parameter generates the Lorentz force which results in the thickening of the momentum boundary layer. Hence, Figure 11 shows the concentration profile increases with increasing Magnetic parameters. Figure 12 shows that increasing the Radiation parameter results in a decrease in the concentration profile. This is because, as the Radiation parameter increases, heat is generated in the flow. An increase in the flow temperature enhances the migration of nanoparticles from the boundary layer and consequently reduces the particle concentration within the boundary layer.

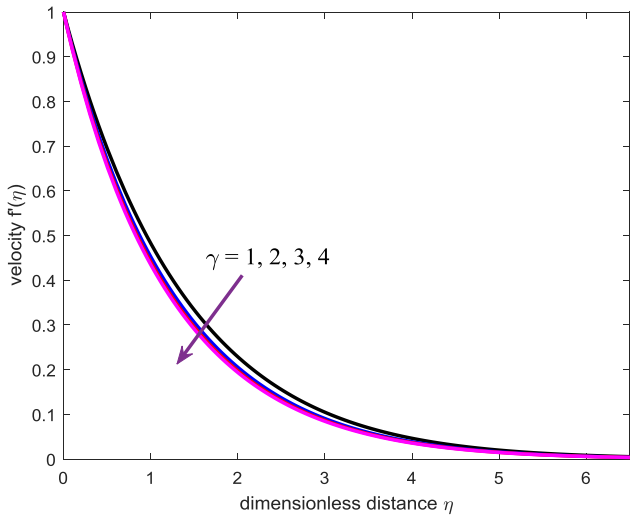

Fig. 2: Primary velocity with Casson parameter

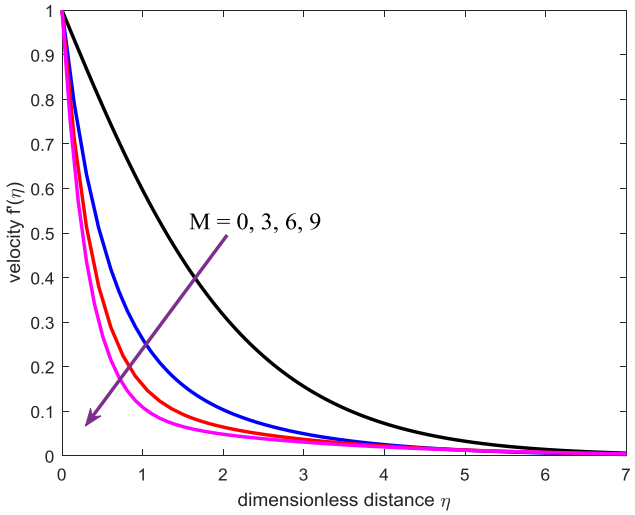

Fig. 3: Primary velocity with Magnetic parameter

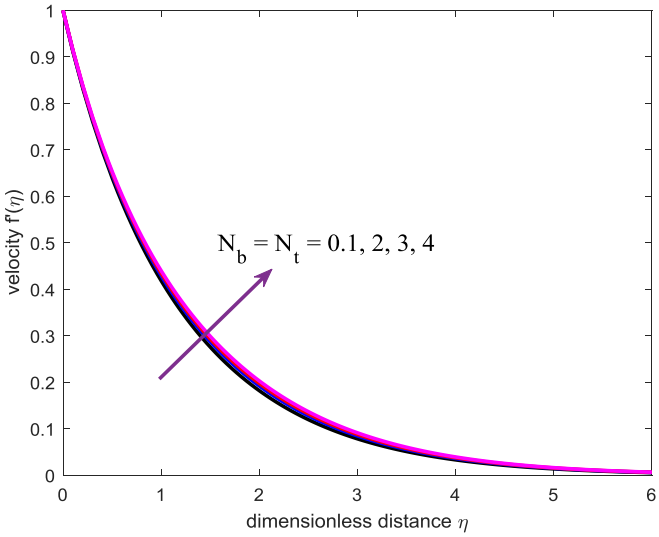

Fig. 4: Brownian motion and Thermophoretic parameters with Primary velocity

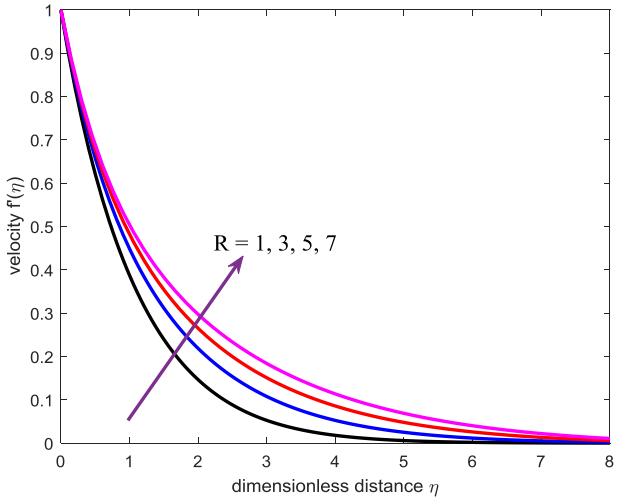

Fig. 5: Primary velocity with Radiation parameter

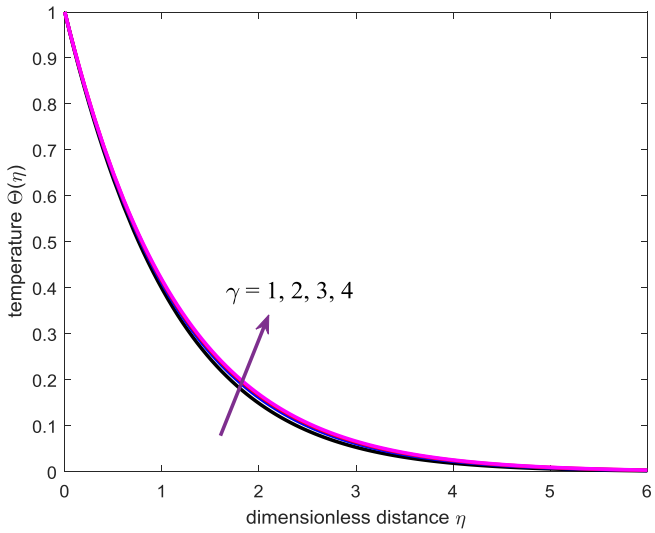

Fig. 6: Temperature with Casson parameter

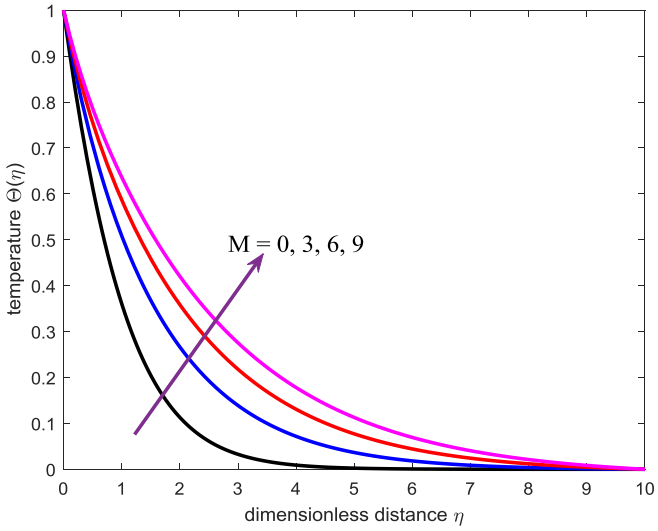

Fig. 7: Temperature with Magnetic parameter

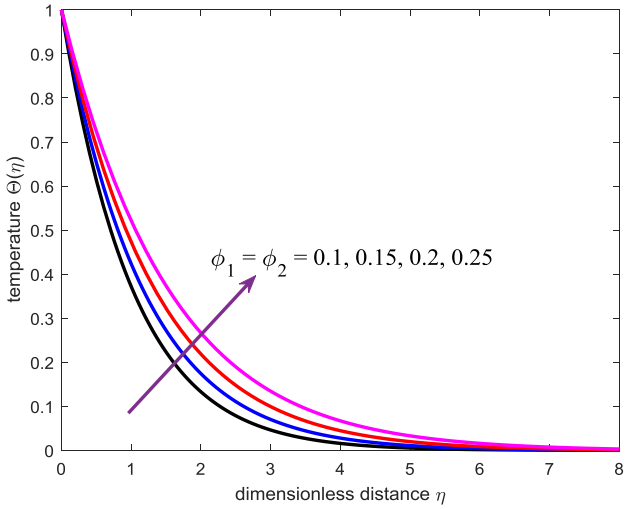

Fig. 8: Temperature with volume fraction

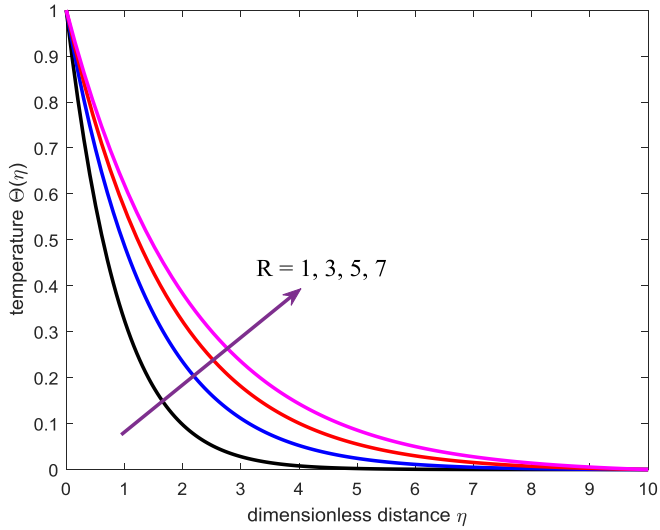

Fig. 9: Temperature with Radiation parameter

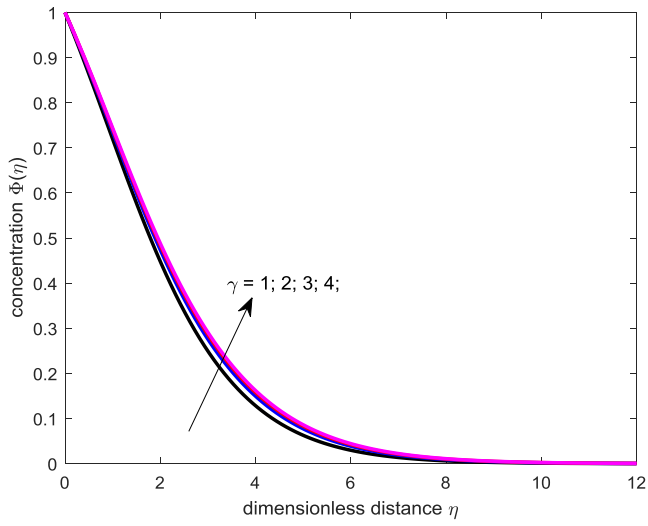

Fig. 10: Concentration with Casson parameter

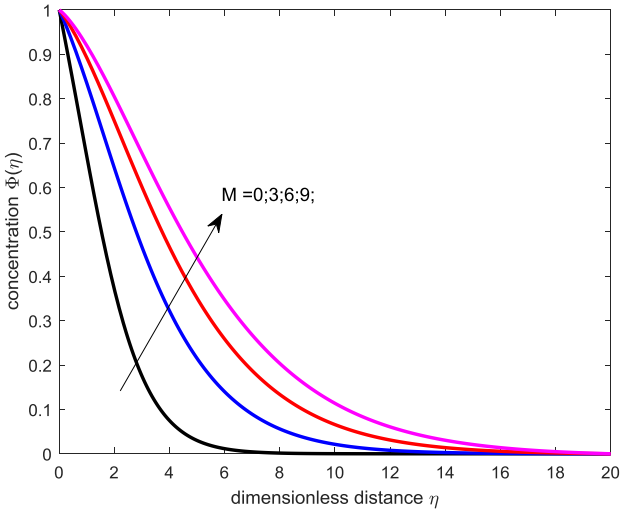

Fig. 11: Concentration with Magnetic parameter

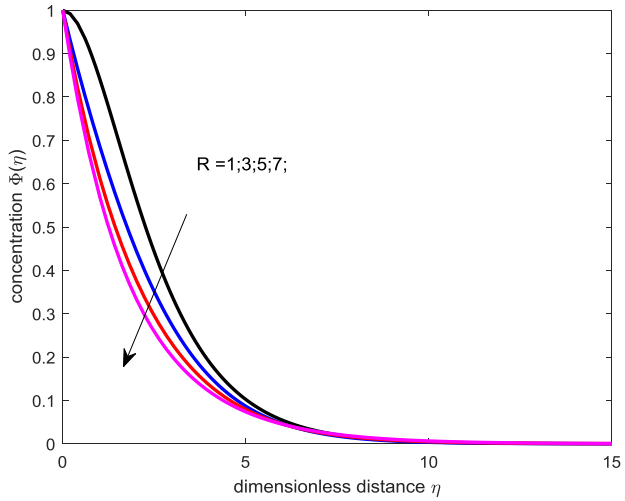

Fig. 12: Concentration with Radiation parameter

4.4 Quantities of Interest

The Skin friction coefficient, Sherwood number, and Nusselt number are computed and shown in Table 3 (Appendix). Local skin friction increases with increasing buoyancy, Casson fluid parameter, and radiation parameter but decreases with increasing magnetic field strength and Prandtl number. The Nusselt number increases with increasing buoyancy and Prandtl number but decreases with increasing magnetic field strength, Casson fluid parameter, and radiation parameter. Sherwood number increases with increasing buoyancy and radiation parameters but decreases with increasing magnetic field strength, Casson fluid parameter, and Prandtl number. By comparing SWCNT water-based nanofluid with the current SWCNT graphene Casson-based hybrid nanofluid, there is a 78.41 percent reduction in skin friction (by comparing the results with, [31]).

5 Conclusion

This study analyses the MHD flow of CNT-Graphene Casson hybrid nanofluid over an ESS. The flow of a hybrid Casson nanofluid is formulated and nondimensionalized using the similarity variables. The effects of pertinent parameters on the flow velocity, flow temperature, and concentration are analyzed and discussed. The results are summarised as follows;

The primary velocity decreases with the Casson fluid parameter and Magnetic field parameter but increases with Brownian motion, Thermophoretic parameter, and Radiation parameter.

1. The temperature profiles increase with the Casson fluid parameter, magnetic field strength, Brownian motion, haphazard motion, volume fraction, and Radiation parameter.
2. The concentration profiles experience an increase with the Casson parameter and Magnetic field strength but a decrease with the Radiation parameter.
3. The Skin friction coefficient increases with the Grashof number, Casson fluid parameter, and radiation parameter but decreases with magnetic field strength and Prandtl number.
4. Nusselt number increases with the Grashof number and Prandtl number but decreases with the Casson fluid parameter, magnetic field strength, and radiation parameter.
5. Sherwood number increases with Grashof number and radiation parameter but decreases with Casson fluid parameter, magnetic field strength, and Prandtl number.

The impact of this paper in modern Fluid Mechanics will be more visible when the thermal conductivity effect is varied alongside other parameters as directions for further research.

References:

[1] A. S. Oke, W. N. Mutuku, M. Kimathi, and I. L. Animasaun. Coriolis effects on MHD Newtonian flow over a rotating non-uniform surface. *Proceedings of the Institution of Mechanical Engineers, Part C: Journal of Mechanical Engineering Science* Vol. 235, No. 19 (2021): 3875-3887.

[2] A. S. Oke, E. O. Fatunmbi, I. L. Animasaun, and B. A. Juma. Exploration of ternary-hybrid nanofluid experiencing Coriolis and Lorentz forces: case of three-dimensional flow of water conveying carbon nanotubes,

graphene, and alumina nanoparticles. *Waves in Random and Complex Media* (2022): 1-20.

[3] A. S. Oke. Combined effects of Coriolis force and nanoparticle properties on the dynamics of gold–water nanofluid across non-uniform surfaces. *ZAMM-Journal of Applied Mathematics and Mechanics/Zeitschrift für Angewandte Mathematik und Mechanik* Vol. 102, No. 9 (2022): e202100113.

[4] A. S. Oke, B. C. Prasannakumara, W. N. Mutuku, R. J. Punith Gowda, B. A. Juma, R. N. Kumar, and O. I. Bada. Exploration of the effects of Coriolis force and thermal radiation on water-based hybrid nanofluid flow over an exponentially stretching plate. *Scientific Reports* Vol. 12, No. 1 (2022): 21733.

[5] Oke, A. S. Theoretical analysis of modified eyring powell fluid flow. *Journal of the Taiwan Institute of Chemical Engineers* Vol. 132 (2022): 104152.

[6] A. S. Oke. Coriolis effects on MHD flow of MEP fluid over a non-uniform surface in the presence of thermal radiation. *International Communications in Heat and Mass Transfer* Vol. 129 (2021): 105695.

[7] A. S. Oke, and W. N. Mutuku. Significance of viscous dissipation on MHD Eyring–Powell flow past a convectively heated stretching sheet. *Pramana* Vol. 95, No. 4 (2021): 199.

[8] A. S. Oke, W. N. Mutuku, M. Kimathi, and I. L. Animasaun. Insight into the dynamics of non-Newtonian Casson fluid over a rotating non-uniform surface subject to Coriolis force. *Nonlinear Engineering*, (2020): 1–17. doi: 10.1515/nleng-2020-0025.

[9] J. O. Ouru, W. N. Mutuku, and A. S. Oke. Buoyancy-induced MHD stagnation point flow of williamson fluid with thermal radiation. *Journal of Engineering Research and Reports*, 2020: 9–18. doi: 10.9734/jerr/2020/v11i417065.

[10] G. W. Scott Blair. An equation for the flow of blood, plasma and serum through glass capillaries. *Nature*, Vol. 183 No. 4661 (1959):613–614.

[11] J. Venkatesan, D. S. Sankar, K. Hemalatha, and Yazariah Yatim. Mathematical analysis of casson fluid model for blood rheology in stenosed narrow arteries. *Journal of Applied Mathematics*, (2013):1–11.

[12] James Clerk Maxwell. A Treatise on Electricity and Magnetism. *Nature*, Vol. 7 (1873):478–480. doi: https: //doi.org/10.1038/007478a0.

[13] U. S. Choi and J.A. Eastman. Enhancing Thermal Conductivity of Fluids with Nanoparticles. *ASME International Mechanical Congress and Exposition, San Francisco*, (1995):12–17.

[14] John Kinyanjui Kigio, Mutuku Winifred Nduku, and Oke Abayomi Samuel. Analysis of Volume Fraction and Convective Heat Transfer on MHD Casson Nanofluid over a Vertical Plate. *Fluid Mechanics*, Vol. 7 No. 1 (2021):1, 2021. doi: 10.11648/j.fm.20210701.11.

[15] A. S. Oke, I. L. Animasaun, W. N. Mutuku, M. Kimathi, Nehad Ali Shah, and S. Saleem. Significance of coriolis force, volume fraction, and heat source/sink on the dynamics of water conveying 47 nm alumina nanoparticles over a uniform surface. *Chinese Journal of Physics*, (2021). ISSN: 0577-9073. doi: 10.1016/j.cjph.2021.02.005.

[16] Bagh Ali, N. Ameer Ahammad, Aziz Ullah Awan, Abayomi S. Oke, ElSayed M. Tag-ElDin, Farooq Ahmed Shah, and Sonia Majeed. The Dynamics of Water-Based Nanofluid Subject to the Nanoparticle's Radius with a Significant Magnetic Field: The Case of Rotating Micropolar Fluid. *Sustainability*, Vol. 14 No. 17 (2022):10474, doi: 10.3390/su141710474.

[17] Suresh, S., K. P. Venkitaraj, P. Selvakumar, and M. Chandrasekar. Synthesis of Al2O3–Cu/water hybrid nanofluids using two step method and its thermophysical properties. *Colloids and Surfaces A: Physicochemical and Engineering Aspects* Vol. 388, no. 1-3 (2011): 41-48.

[18] Hayat, Tanzila, and S. Nadeem. "Heat transfer enhancement with Ag–CuO/water hybrid nanofluid." *Results in physics,* Vol. 7 (2017): 2317-2324.

[19] John A. Okello, Anselm O. Oyem, and Winifred N. Mutuku. Examination of engine oil-based ((MWCNTs-TiO_2), (MWCNTs-Al_2O_3), (MWCNTs-Cu)) hybrid nanofluids for optimal nanolubricant. *Journal of Mathematics (IOSR-JM)*, Vol. 17, No. 2 (2021):24–38. doi.org/10.9790/5728-1702012438.

[20] Sheid A. MomohJimoh, Oyem O. Anselm, Momoh O. Sheidu, and Onojovwo T. Felix. Convective heat and Casson nanofluid flow over a vertical plate with heat sources. *FUDMA Journal of Sciences*, Vol. 7, No. 2

(2023):9–18. doi.org/10.33003/fjs-2023-0702-1398.

[21] Onojovwo T. Felix, Oyem O. Anselm, Momoh O. Sheidu, and Sheid A. MomohJimoh. Casson nanofluid over a vertical plate and its thermophysical properties. *FUW Trends in Science & Technology Journal*, Vol. 8 No. 2 (2023):044–051: e-ISSN: 24085162; 82FTSTJ0072023.

[22] Subhani, Maryam, and Sohail Nadeem. "Numerical analysis of micropolar hybrid nanofluid." *Applied Nanoscience* Vol. 9 no. 4 (2019): 447-459.

[23] M. Sheikholeslami, S.A.M. Mehryan, Ahmad Shafee, and Mikhail A. Sheremet. Variable magnetic forces impact on magnetizable hybrid nanofluid heat transfer through a circular cavity. *Journal of molecular liquids* Vol. 277 (2019): 388–396.

[24] Waini, Iskandar, Anuar Ishak, and Ioan Pop. Unsteady flow and heat transfer past a stretching/shrinking sheet in a hybrid nanofluid. *International Journal of Heat and Mass Transfer* Vol. 136 (2019): 288-297.

[25] Zainal, Nurul Amira, Roslinda Nazar, Kohilavani Naganthran, and Ioan Pop. "MHD flow and heat transfer of hybrid nanofluid over a permeable moving surface in the presence of thermal radiation." *International Journal of Numerical Methods for Heat & Fluid Flow* Vol. 31, No. 3 (2021): 858-879.

[26] Tassaddiq, Asifa, Sadam Khan, Muhammad Bilal, Taza Gul, Safyan Mukhtar, Zahir Shah, and Ebenezer Bonyah. "Heat and mass transfer together with hybrid nanofluid flow over a rotating disk." *AIP Advances* Vol. 10, no. 5 (2020).

[27] Othman, Mohamad Nizam, Alias Jedi, and Nor Ashikin Abu Bakar. MHD Flow and Heat Transfer of Hybrid Nanofluid over an Exponentially Shrinking Surface with Heat Source/Sink" *Applied Sciences* Vol. 11 No. 17 (2021), no. 17: 8199.

[28] Mahantesh M. Nandeppanavar, M. C. Kemparaju, and N. Raveendra. Effect of Richardson number on double-diffusive mixed convective slip flow, Heat and Mass transfer of MHD Casson fluid. *Proceedings of the Institution of Mechanical Engineers, Part E: Journal of Process Mechanical Engineering*, (2022):095440892210792. doi: 10.1177/09544089221079264.

[29] Mulat Alubel Abtew, François Boussu, and Pascal Bruniaux. Dynamic impact protective body armour: A comprehensive appraisal on panel engineering design and its prospective materials. *Defence Technology*, Vol. 17 No.6 (2021):2027–2049, doi: 10.1016/j.dt.2021.03.016.

[30] Jesuarockiam Naveen, Mohammad Jawaid, Kheng Lim Goh, Degalhal Mallikarjuna Reddy, Chandrasekar Muthukumar, Tamil Moli Loganathan, and Koduri Naga Ganapathy Lakshmi Reshwanth. Advancement in Graphene-Based Materials and Their Nacre Inspired Composites for Armour Applications - A Review. *Nanomaterials*, Vol. 11 No. 5(2021):1239. doi: 10.3390/nano11051239.

[31] Zakir Hussain, Tasawar Hayat, Ahmed Alsaedi, and Muhammad Shoaib Anwar. Mixed convective flow of CNTs nanofluid subject to varying viscosity and reactions. *Scientific Reports*, Vol. 11 No. 1 (2021). doi: 10.1038/s41598-021-02228-9.

[32] Ali Rehman, Zabidin Salleh, and Taza Gul. Influence of dynamics viscosity on the water base CNTs nanofluid flow over a stretching surface. *Cogent Engineering*, Vol. 7 No.1 (2020):1772945. doi: 10.1080/23311916. 2020.1772945.

[33] J. Buongiorno. Convective Transport in Nanofluids. *Journal of Heat Transfer*, Vol. 128 No. 3(2005): 240–250. doi: 10.1115/1.2150834.

[34] Belindar A. Juma, Abayomi S. Oke, Winifred N. Mutuku, Afolabi G. Ariwayo, and Olum J. Ouru. Dynamics of Williamson fluid over an inclined surface subject to Coriolis and Lorentz forces. *Engineering and Applied Science Letters*, Vol. 5, No. 1 (2022): 37–46. doi:10.30538/psrp-easl2022.0083.

[35] A. S. Oke. Convergence of differential transform method for ordinary differential equations. *Journal of Advances in Mathematics and Computer Science*, Vol. 24 No. 6 (2017):1–17.

[36] Muhammad Bilal, Hamna Arshad, Muhammad Ramzan, Zahir Shah, and Poom Kumam. Unsteady hybrid-nanofluid flow comprising ferrousoxide and CNTs through porous horizontal channel with dilating/squeezing walls. *Scientific Reports*, Vol. 11 No.1 (2021):12637. ISSN: 2045-2322. doi: 10.1038/ s41598-021-91188-1.

[37] Syed M. Hussain, Rohit Sharma, Manas R. Mishra, and Sattam S. Alrashidy. Hydromagnetic Dissipative and Radiative Graphene Maxwell Nanofluid Flow Past a Stretched Sheet-Numerical and Statistical Analysis. *Mathematics*, Vol. 8 No. 11 (2020). ISSN: 2227-7390. doi: 10.3390/math8111929.

[38] Volodymyr M. Nahirnyak, Suk Wang Yoon, and Christy K. Holland. Acousto-mechanical and thermal properties of clotted blood. *The Journal of the Acoustical Society of America*, Vol. 119 No. 6 (2006):3766–3772. doi: 10.1121/1.2201251.

APPENDIX

Table 3. Quantities of Engineering Interests

Gr	M	γ	Pr	R	$Re^{\frac{1}{2}}C_f$	$Re^{-\frac{1}{2}}Nu$	$Re^{-\frac{1}{2}}Sh$
0.5 2 3.5 5	1				-1.245633315 -0.581040882 ↑ 0.013917089 0.569252613	0.817985874 0.917571328 ↑ 0.980956426 1.029835214	0.175714756 0.263425671 ↑ 0.312889511 0.348744744
1	0.5 2 3.5 5	10			-0.770475997 -1.416580567 ↓ -1.904957996 -2.310164241	0.89768154 0.794891068 ↓ 0.721866343 0.666172034	0.251527008 0.160088346 ↓ 0.113210799 0.087029664
	1	0.5 2 3.5 5	7.2		-1.878560408 -1.226410213 ↑ -1.11489622 -1.068341673	0.914037518 0.875955507 ↓ 0.867363509 0.863537079	0.273490546 0.229718612 ↓ 0.22127766 0.217717838
		10	0.5 2 3.5 5	2	-0.798933832 -0.880842247 ↓ -0.931761986 -0.969721143	0.195647542 0.407504098 ↑ 0.562481803 0.692952712	0.81439048 0.642261504 ↓ 0.500400584 0.375550069
			7.2	0.5 2 3.5 5	-1.104480262 -1.012422753 -0.965114487 ↑ -0.934952758	1.299137965 0.858737594 0.680157903 ↓ 0.578255755	-0.22112938 0.213431548 0.388498895 ↑ 0.486205056

Nomenclature

Variables and parameters			
u, v	Velocity components along the x, y-axes	C_f	Skin friction coefficient
T_w, T_∞	Temperature at the wall and free stream	ρ	Density coefficient
C_w, C_∞	Concentration at the wall and free stream	c_p	Specific heat capacity
T	Temperature	α	Thermal diffusivity
C	Concentration	L	Characteristic length
ν, μ	Dynamic and Kinematic viscosity	ϕ	Volume fraction
q, q_w	Radiative and wall heat flux	Pr	Prandtl number
β	Thermal expansion coefficient	Gr	Grashof number
σ	Electric conductivity coefficient	Re	Reynold number
g	Acceleration due to gravity	Sh	Sherwood number
B_0	Magnetic field strength	Nu	Nusselt number
D_T, D_B	Thermophoretic and Brownian diffusivity	Sc	Schmidt number
K	Thermal conductivity	M	Magnetic parameter
σ^*	Stefan-Boltzmann constant	γ	Casson fluid parameter
N_b	Brownian motion parameter	R	Radiation parameter
N_t	Thermophoretic parameter	f'	dimensionless velocity
K^*	Mean absorption coefficient	η	dimensionless distance
Θ	dimensionless temperature	Φ	dimensionless concentration

subscripts	
hnf = hybrid nanofluid	1 = carbon nanotubes-Casson fluid nanofluid
f = base Casson fluid	2 = graphene-Casson fluid nanofluid

Contribution of Individual Authors to the Creation of a Scientific Article (Ghostwriting Policy)

The authors equally contributed to the present research, at all stages from the formulation of the problem to the final findings and solution.

Sources of Funding for Research Presented in a Scientific Article or Scientific Article Itself

No funding was received for conducting this study.

Conflict of Interest

The authors have no conflicts of interest to declare.